

# 1 **Evaluation of open and closed path sampling systems for determination**

## 2 **of emission rates of NH<sub>3</sub> and CH<sub>4</sub> with inverse dispersion modelling**

3 Yolanda Maria Lemes<sup>a</sup>, Christoph Häni<sup>b</sup>, Jesper Nørlem Kamp<sup>a</sup>, Anders Feilberg<sup>\*a</sup>

4 <sup>a</sup>Department of Biological and Chemical Engineering, Aarhus University, Gustav Wieds Vej 10D, 8000 Aarhus,  
5 Denmark.

6 <sup>b</sup>School of Agricultural, Forest and Food Sciences, Bern University of Applied Sciences, Länggasse 85, 3052  
7 Zollikofen, Switzerland

8 *\*Corresponding author: email: af@bce.au.dk; Telephone: +45 30896099*

9 Declaration of interest: none

### 10 **Abstract**

11 The gas emission rates of ammonia (NH<sub>3</sub>) and methane (CH<sub>4</sub>) from an artificial source covering a surface  
12 area of 254 m<sup>2</sup> were determined by inverse dispersion modelling (IDM) from point and line-integrated  
13 concentration measurements with closed and open-path analyzers. Eight controlled release experiments  
14 were conducted with different release rates ranging from  $3.8 \pm 0.21$  to  $17.4 \pm 0.4$  mg s<sup>-1</sup> and from  $30.7 \pm$   
15  $1.4$  to  $142.8 \pm 2.9$  mg s<sup>-1</sup> for NH<sub>3</sub> and CH<sub>4</sub>, respectively. The distance between the source and  
16 concentration measurement positions ranged from 15 m to 60 m. Our study consisted of more than 200  
17 fluxes averaged over intervals of 10 min or 15 min. The different releases cover a range of different  
18 climate conditions: cold (< 5°C), temperate (< 13 °C) and warm (< 18 °C). As the average of all releases  
19 with all instrument types, the CH<sub>4</sub> recovery rate  $Q_{\text{BLS}}/Q$  was  $0.95 \pm 0.08$  (n = 19). There was much more  
20 variation in the recovery of NH<sub>3</sub>, with an average of  $0.66 \pm 0.15$  (n = 10) for all the releases with the line-  
21 integrated system. However, with an improved sampling line placed close to the source an average  
22 recovery rate of  $0.82 \pm 0.05$  (n = 3) was obtained for NH<sub>3</sub>. Under comparable conditions, the recovery  
23 rate obtained with an open-path analyzer was  $0.91 \pm 0.07$  (n = 3). The effects of measurement distance,  
24 physical properties of the sampling line, and deposition are discussed.

25 **Keywords:** Method validation, Ammonia, Methane, Inverse Dispersion Method, Backward Lagrangian  
26 Stochastic, bLS

## 27 **1 Introduction**

28 The global agricultural system is currently facing one of its biggest humanitarian challenges:  
29 feeding the world's rising population while preserving the environment and climate for future generations  
30 (FAO, 2017). The agricultural sector is a major contributor to global greenhouse gas (GHG) emissions  
31 (15%) and ammonia (NH<sub>3</sub>) emissions (64%) (OECD and FAO, 2019), leading to air pollution, climate  
32 change, deforestation, and loss of biodiversity (Aneja et al., 2009).

33 The European Union has established a reduction target for 2030 to reduce the GHG emissions by at  
34 least 55% (EEA, 2019), compared to 1990, and NH<sub>3</sub> emissions by 19% (NEC Directive 2016/2284),  
35 compared to 2005. Agriculture must contribute to GHG emission reductions, and valid estimates of GHG  
36 emissions are important for national inventories regulation strategies and for selecting efficient mitigation  
37 techniques.

38  
39 Choosing the appropriate methodology to quantify gaseous emissions can be a challenge. In  
40 particular agricultural sources are challenging as the sources often are small and inhomogeneous, exhibit  
41 non-steady emissions over time (e.g. NH<sub>3</sub> emissions after slurry application (Hafner, 2018)) and are  
42 influenced by other sources in close vicinity. Most of the methodologies have restrictions on the  
43 measurement location and/or the source and involve complex instrumentation set-up (e.g., fast-response  
44 analyzers, measurements at multiple heights). The micrometeorological mass balance (MMB) method  
45 (Desjardins et al., 2004) requires measuring concentration at multiple positions several meters above the  
46 ground, which is a challenge for obtaining high time resolution and it ignores the horizontal turbulent  
47 transport (Hu et al., 2014). The tracer flux ratio method (TRM), which has also been used to measure  
48 agricultural emissions (Vechi et al., 2022; Fredenslund et al., 2019; Delre et al., 2018), is a relatively

49 labor intensive and costly method typically with short intense measurement periods. In case of dynamic  
50 emissions, this is not sufficient for resolving the temporal variations in emissions over days or weeks.

51 The inverse dispersion method (IDM) based on backward Lagrangian Stochastic (bLS) dispersion  
52 modelling (e.g. Flesch et al., 2004, 1995) has been widely used for the assessment of NH<sub>3</sub> and methane  
53 (CH<sub>4</sub>) emissions from many agricultural sources: dairy housing (Bühler et al., 2021; VanderZaag et al.,  
54 2014; Harper et al., 2009), cattle feedlot (McGinn et al., 2019; Todd et al., 2011; van Haarlem et al.,  
55 2008; Flesch et al., 2007; McGinn et al., 2007), application of liquid animal manure (Kamp et al., 2021;  
56 Carozzi et al., 2013; Sintermann et al., 2011; Sanz et al., 2010), grazed pasture (McGinn et al., 2011;  
57 Voglmeier et al., 2018), rice field (Yang et al., 2019), lagoon (Ro et al., 2014; Wilson et al., 2001),  
58 composting stockpiles (Sommer et al., 2004), agricultural biodigester (Baldé et al., 2016b; Flesch et al.,  
59 2011), farm (Flesch et al., 2005) and stored liquid manure (Lemes et al., 2022; Baldé et al., 2016a; Grant  
60 et al., 2015; McGinn et al., 2008).

61 IDM has been tested in controlled release experiments with different conditions: ground level  
62 source without obstacles (Flesch et al., 2014; McBain and Desjardins, 2005a; Flesch et al., 2004), ground  
63 level source surrounded by a fence (Flesch et al., 2005; McBain and Desjardins, 2005a), elevated source  
64 (Gao et al., 2008; McBain and Desjardins, 2005a), multiple emission sources (Hu et al., 2016; Ro et al.,  
65 2011; Gao et al., 2008) and to quantify the effect of NH<sub>3</sub> deposition (Häni et al., 2018).

66 IDM is a function of the geometry and location of source and downwind concentration sensor  
67 (including height for the sensor) and the turbulence characteristics in the surface layer. The statistical  
68 properties of the flow in the atmospheric surface layer for the IDM are defined by the friction velocity  
69 ( $u^*$ ), roughness length ( $z_0$ ), the Obukhov length ( $L$ ), and wind direction (Flesch et al., 2004). Emissions  
70 are derived from concentration measurements up- and downwind of the source, which could be  
71 determined with point or line-integrated measurements from closed- or open-path analyzers. IDM  
72 assumes an ideal atmospheric surface layer, which means i) a horizontally homogeneous and flat surface,

73 ii) homogeneity and quasi-stationarity with respect to the turbulence characteristics and iii) spatially  
74 uniform emissions from a confined source (Flesch et al., 2004). Therefore, there should not be any  
75 obstacles (e.g., trees, buildings) in close vicinity of the source to fulfil the required IDM assumptions.  
76 Additionally, IDM has the limitation that there should not be any other sources of the same gas species  
77 that affects up- and downwind concentration differently. The IDM is simple, flexible (Harper et al.,  
78 2011), robust even in non ideal conditions and has a reported accuracy of  $100 \pm 10\%$  when it is properly  
79 used (e.g., place of instruments, filtering criteria) (Harper et al., 2010). Moreover, IDM is a direct  
80 measurement method that does not alter the physical properties of the source, and it is applicable for both  
81 small and large emissions of any shape of sources (Flesch et al., 2004) as opposed to indirect enclosure  
82 methods (e.g. chambers measurements).

83 Concentration measurements are mostly done with an open-path optical system (e.g. Baldé et al.,  
84 2018; Bühler et al., 2021) because long path lengths (>50 m) enable a higher emission plume coverage  
85 and avoids internal surfaces (e.g. tubes, pumps) where  $\text{NH}_3$  can adsorb (Shah et al., 2006; Vaittinen et al.,  
86 2014). However, open-path has a limitation on low concentration measurements (<10 ppb for  $\text{CH}_4$  and  
87  $\text{NH}_3$ ) (Bai et al., 2022) and requires complex calibrations to reduce the uncertainty of the measurements  
88 (Häni et al., 2021; DeBruyn et al., 2020). In addition, it requires intensive labor to move and optically  
89 align the instruments to different positions depending on the predominant wind direction. Commercially  
90 available open-path analyzers exhibit limitations with respect to acceptable detection limits (Häni et al.,  
91 2021). Closed-path analyzers have rarely been used together with the IDM (Ro et al., 2011) due to its  
92 limitation caused by adsorption of  $\text{NH}_3$  in the system. In addition, closed path analyzers have only been  
93 used for point measurements, which challenges the ability to catch the emission plume and makes it  
94 sensitive to wind direction accuracy.

95 Data filtering is needed to ensure accuracy of the IDM, which is related to the meteorological  
96 conditions (e.g., wind speed, atmospheric stability) and wind direction. The quality criteria for filtering  
97 are based on the atmospheric conditions in a measurement interval to ensure the assumptions of the model

98 is adequately met, which also lower the uncertainty of the resulting data. Different criteria have been used  
99 in previous studies: Flesch et al. (2005) recommend to remove data where  $u^* < 0.15 \text{ m s}^{-1}$ ,  $|L| < 10 \text{ m}$  and  
100  $z_0 > 1 \text{ m}$ , whereas McBain and Desjardins, 2005 recommend  $u^* < 0.19 \text{ m s}^{-1}$ ,  $|L| \leq 3 \text{ m}$  and  $z_0 > 1 \text{ m}$ .  
101 Flesch et al. (2014) suggest the filtering criteria for the night of  $u^* < 0.05 \text{ m s}^{-1}$  and the gradient between  
102 measured and MO-calculated temperature ( $|\Delta\Delta T|_{\text{thres}} = 0.05 \text{ K}$ ). Bühler et al. (2021) removed data  
103 where  $u^* < 0.05 \text{ m s}^{-1}$ ,  $|L| < 2 \text{ m}$ ,  $z_0 > 0.1 \text{ m}$ , standard deviation of the horizontal wind components ( $u, v$ )  
104 divided by  $u^*(\sigma_{u,v}/u^*) > 4.5$  and Kolmogorov constant ( $C_0 > 10$ ).

105 This study aimed to assess the applicability and performance of a closed-path analyzer used with a  
106 sampling system that allows for line integrated concentration measurements used with the IDM for  
107 determining emission rates of  $\text{CH}_4$  and  $\text{NH}_3$ . This novel measuring system will allow for measuring  
108 emissions from sources with low emission rates and will have good flexibility for moving it around the  
109 source depending on the wind direction in order to increase the probability of catching the emission  
110 plume. This novel method is assessed by eight controlled releases of  $\text{CH}_4$  and  $\text{NH}_3$  combined with up- and  
111 downwind measurements in different positions using point and line-average concentration provided with  
112 closed- and open-path analyzers. The use of  $\text{CH}_4$  and  $\text{NH}_3$  and open- and closed-path systems to measure  
113 concentration will give us an opportunity to: i) test the system of the line-average concentration  
114 measurement with a closed-path analyzer; and ii) evaluate potential loss of  $\text{NH}_3$  downwind from the  
115 source by deposition and/or gas-to-particle conversion, processes that will not occur for inert  $\text{CH}_4$ . This  
116 controlled-release study is the first to compare the performances of open-path and line-integrated closed-  
117 path systems for measuring emissions of  $\text{NH}_3$  and  $\text{CH}_4$ .

118

## 119 2 Material and methods

### 120 2.1 Site descriptions

121 From November 2019 to March 2022, eight controlled release experiments were performed at  
122 different grassland sites under varying conditions (see Table 1). Five releases (I-DK to IV-DK and VIII-  
123 DK) took place at AU campus Viborg, Denmark on two different fields (56°29'34.5"N / 9°34'28.3"E and  
124 56°29'36.4"N / 9°34'15.9"E). Three releases (V-CH to VII-CH) were performed at Bern University of  
125 Applied Sciences, Switzerland (46°59'35.1"N / 7°27'43.1"E). At all sites, the terrain was horizontally flat,  
126 and the height of the canopy varied between 15 and 25 cm for the different experiments. Obstacles upwind  
127 of the artificial source were more than 100 m away in all experiments. There were no significant sources  
128 near the experiment sites.

### 129 2.2 Instrumentation

130 In this study, different models of cavity ring-down spectroscopy (CRDS) analyzers from Picarro  
131 (Picarro Inc., Santa Clara, CA, USA) were used to measure up- and downwind NH<sub>3</sub> and CH<sub>4</sub> concentration  
132 (Table 1). Model G2201-i and model G4301 measure CH<sub>4</sub> concentration, G2103 measures NH<sub>3</sub>  
133 concentration, and G2509 measures CH<sub>4</sub> and NH<sub>3</sub> simultaneously. The CRDS is a closed-path analyzer with  
134 continuous absorption that measures concentrations at approximately 0.5 Hz. The CRDS analyzer consists  
135 of a laser and an optical cavity chamber with highly reflective mirrors, which gives an effective path length  
136 of several kilometers. The light is absorbed in the cavity, and the decay of light intensity is called the ring-  
137 down time, which is directly related to the concentration of the specific compound. It has been frequently  
138 used to study agricultural emissions (e.g., Kamp et al., 2021; Pedersen et al., 2020; Kamp et al., 2019;  
139 Sintermann et al., 2011). Calibration of these CRDS instruments are conducted using a certified standard  
140 gas and a dilution system with NH<sub>3</sub> free air before each release. Mass flow controllers (Bronkhorst EL  
141 FLOW, Ruurlo, Netherlands) were used to obtain a range of desired concentrations in all calibrations. The  
142 standard gas contained 10±0.31 ppm NH<sub>3</sub> (Air Liquide, Horsens, Denmark) and 100±2 ppm CH<sub>4</sub> (Air  
143 Liquide, Horsens, Denmark). Calibration showed high linearity of the instruments with  $R^2 = 1$ . The CRDS

144 instruments used pairwise for upwind and downwind measurements agreed within  $\pm 5\%$  and no correction  
145 of the instruments were therefore done, see Figure S5 and Figure S6 in the Supplementary Information.

146 In experiments V-CH to VII-CH, the downwind  $\text{CH}_4$  concentration was measured with three  
147 GasFinder3 analyzers (GF3, Boreal Laser Inc., Edmonton Canada) and the downwind  $\text{NH}_3$  concentration  
148 with three miniDOAS instruments (Sintermann et al., 2016). The GF3 analyzer is an open-path tunable  
149 diode laser device that measures line-integrated  $\text{CH}_4$  concentrations over path lengths of 5 to 500 m (i.e.  
150 single path length between sensor and retroreflector) with a temporal resolution of 0.3 to 1 Hz. The  
151 retroreflectors used in the experiments were equipped with seven corner cubes, suitable for path lengths  
152 around 50 m. The GasFinder devices have been widely used to measure emissions from different type of  
153 agricultural sources with the IDM (Bühler et al., 2021; McGinn et al., 2019; VanderZaag et al., 2014; Harper  
154 et al., 2010; Flesch et al., 2007). The performance of the GF3 instruments is discussed in detail by Häni et  
155 al. (2021). The GF3 instrument were intercompared with the calibrated CRDS instrument by measuring  
156 ambient concentrations over at least one day and corrected accordingly. The applied corrections were  $c =$   
157  $c_{GF} + 0.14$ ,  $c = c_{GF} + 0.22$ ,  $c = c_{GF} + 0.12$  for the GF3 placed 15 m, 30 m, and 60 m from the source,  
158 respectively.

159 The miniDOAS instrument is an open-path device that measures  $\text{NH}_3$ ,  $\text{NO}$  and  $\text{SO}_2$  in the UV region  
160 between 190 and 230 nm based on the differential optical absorption spectroscopy (DOAS; Platt and Stutz,  
161 2008) technique. It provides path-averaged concentrations for path lengths between 15 m and 50 m, with  
162 around 10 to 20 scans per second averaged over 1 minute. Ammonia emissions from agricultural sources  
163 (Kamp et al., 2021; Kupper et al., 2021; Voglmeier et al., 2018) and from an artificial source (Häni et al.,  
164 2018) have been measured with miniDOAS analyzers. Further details on the instrument is given in  
165 Sintermann et al. (2016). The miniDOAS instruments were intercompared with the calibrated CRDS  
166 instrument by measuring ambient concentrations over at least one day. The miniDOAS offset concentration  
167 from the reference period 08-10-2021 from 15:30 to 17:00 was added ( $3.2 \mu\text{g m}^{-3}$ ).

168 2.3 Gas release from an artificial source

169 The artificial source area had a gas distributor unit at the center and eight 1/4" polytetrafluoroethylene  
 170 (PTFE) tubes leave the distributor to get a circular shape of the source area. Each tube contained three  
 171 critical orifices (100  $\mu\text{m}$  diameter, stainless steel, LenoxLaser, USA) in series with 3 m distance between  
 172 them. In total, the 24 orifices covered a circular area of 254  $\text{m}^2$ .

173 Gas was released from a gas cylinder and the flow was controlled with a mass flow controller (in  
 174 Denmark: Bronkhorst EL FLOW, Ruurlo, Netherlands; in Switzerland: red-y smart controller, Voegtlin  
 175 Instruments GmbH, Aesch, Switzerland). The source height, the content of the gas cylinders, and the release  
 176 rate for each experiment are given in Table 1.

177 **Table 1** Date, gas cylinders description, ammonia and methane release rate (RR), source and canopy height, downwind  
 178 distance from source to instruments, type of system attached to the cavity ring-down spectroscopy (CRDS), and  
 179 instrumentation of each controlled release experiment (CRE). G2103, G2202-i, G4301 and G2508 are different CRDS  
 180 models, GF correspond to GasFinder and MD to miniDOAS.

CRE	Date	Gas cylinder			NH <sub>3</sub> RR	CH <sub>4</sub> RR	Source height	Canopy height	Distance from source edge	System with CRDS	Instruments
		Content	[bar]	total	[mg s <sup>-1</sup> ]	[mg s <sup>-1</sup> ]	[cm]	[cm]	[m]		
I-DK	29-11-2019 11:50 – 12:50	5% NH <sub>3</sub> and 95% N <sub>2</sub> $\pm$ 2%*	62	1	4.6 $\pm$ 0.3	-	0	20	50	Point 40°C	2 G2103
II-DK	29-11-2019 14:00-14:30	99% CH <sub>4</sub> and 1% N <sub>2</sub> $\pm$ 2%*	62	1	-	30.7 $\pm$ 1.4	0	20	50	Point 40°C	G2201-i and G4301
III-DK	12-10-2020 11:45-15:15	5% NH <sub>3</sub> and 95% CH <sub>4</sub> $\pm$ 2%*	62	1	3.8 $\pm$ 0.21	68.7 $\pm$ 3.7	0	25	35 - 60	16m line 40°C (Line 1)	G2103, G4301 and G2508
IV-DK	20-07-2021 10:30-16:00	10% NH <sub>3</sub> and 90% CH <sub>4</sub> $\pm$ 2%*	62	2	17.4 $\pm$ 0.4	142.8 $\pm$ 2.9	50	18	15-30	12m line 40°C (Line 2)	G2103, G4301 and G2508
V-CH	09-10-2021 10:00-12:10	10% NH <sub>3</sub> and 90% CH <sub>4</sub> $\pm$ 2% <sup>+</sup>	27	2	15.2 $\pm$ 0.3	128.9 $\pm$ 2.7	0	15	15 - 30 - 60	16m line 40°C (Line 1)	G4301, G2508, 3 GF and 3 MD
VI-CH	09-10-2021 14:20-16:50	10% NH <sub>3</sub> and 90% CH <sub>4</sub> $\pm$ 2% <sup>+</sup>	27	4	13.2 $\pm$ 0.3	111.8 $\pm$ 2.2	0	15	15 - 30 - 60	16m line 40°C (Line 1)	G4301, G2508, 3 GF and 3 MD
VII-CH	09-10-2021 17:20-17:50 11-10-2021 15:10-16:20	10% NH <sub>3</sub> and 90% CH <sub>4</sub> $\pm$ 2% <sup>+</sup>	27	4	13.2 $\pm$ 0.3	111.8 $\pm$ 2.2	50	15	15 - 30 - 60	16m line 40°C (Line 1)	G4301, G2508, 3 GF and 3 MD



VIII-DK	22-04-2022 12:30-15:00	10% NH <sub>3</sub> and 90% CH <sub>4</sub> ± 2%*	62	2	14.5± 0.3	118.9 ± 2.8	50	7	15	12m line 40°C (Line 2)and 12m line 80°C with heated inlets (Line 3)	3 G2508
*Air Liquide, Horsens, Denmark											
†Carbagas, Bern, Switzerland											

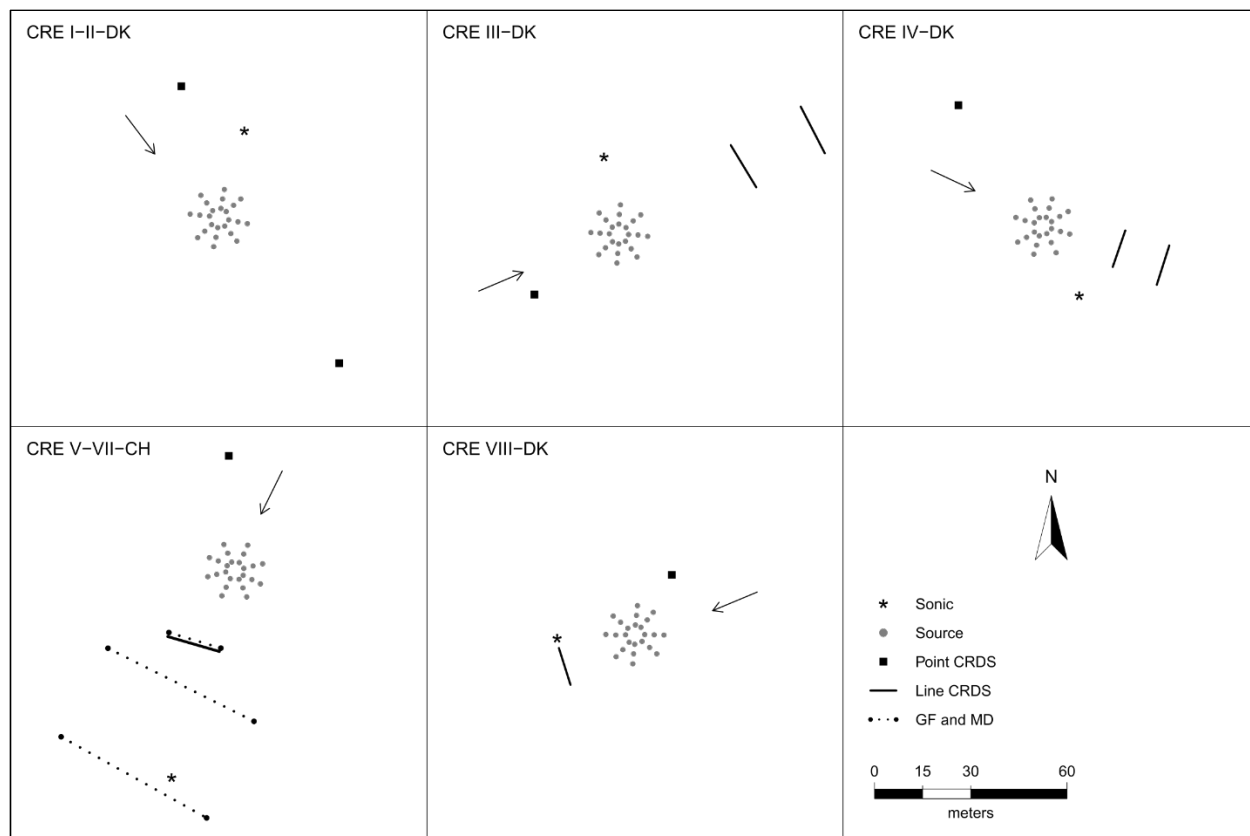
181

## 182 2.4 Set-up

183 In the upwind position of all the experiments and in the downwind position of the I-DK and II-DK  
184 experiment, the CRDS measured the concentration from a single point 1.5 m above ground through a  
185 polytetrafluoroethylene (PTFE) tube that was insulated and heated to approximately 40°C. In the rest of the  
186 experiments, the CRDS measured downwind concentration from a sampling line system of PTFE tubes-  
187 (Line 1 and Line 2) and polyvinylidene fluoride (PVDF) tube (Line 3) insulated and heated (40°C or 80°C).  
188 The difference between the point and line-integrated system is the number of positions where the gas sample  
189 is taken from. The point system had only one inlet, while the line-integrated had several. Three different  
190 versions of the line-integrated system (line) were built and used during this research. In the III-DK, V-DK,  
191 VI-CH, and VII-CH experiment, the sampling line system consisted of a 16 m tube with nine inlets, 2 m  
192 between each inlet (Line 1). In the IV-DK and VIII-DK experiment, the sampling lines were 12 m long  
193 with seven inlets, 2 m between each inlet (Line 2 and Line 3). The inlets are made of critical orifices (0.25  
194 mm ID for I-DK to VII-CH and 0.5 mm ID for VIII-DK polyetheretherketone (PEEK)) that guarantee  
195 uniform flow through each inlet (Line 1, Line 2 and Line 3). In the VIII-DK experiment, the sampling line  
196 system including the inlets was heated to 80°C (Line 3).

197 Figure 1 shows the position of the source area relative to the sampling position and the arrow  
198 indicates the wind direction during the experiments. The downwind concentrations were measured in one,  
199 two or three distance (Table 1). In the V-CH, VI-CH and VII-CH, downwind concentrations were measured  
200 at the same time at 15 m, 30 m and 60 m distance from the edge of the source with multiple GF3 and  
201 miniDOAS instruments; one CRDS instrument was placed 15 m downwind (Figure 1). The distance  
202 between the reflector and the laser/detector of the GF3 and miniDOAS at the downwind position parallel  
203 to the CRDS sampling line was also 16 m. For the other two downwind positions the path lengths were 15  
204 m and 50 m, respectively. The height of the measurement paths of all the open-path instruments were  
205 between 1.2 and 1.5 m. The background concentration of NH<sub>3</sub> was stable with no sources in close vicinity,  
206 thus in the three experiments, the average concentration of each instrument 10 min before the release of

207 each experiment was used as the NH<sub>3</sub> upwind concentration for the miniDOAS and the CRDS instruments.  
 208 In the V-CH, VI-CH and VII-CH experiment, the measured NH<sub>3</sub> background concentration was 2.7 and 4.1  
 209 mg m<sup>-3</sup>, and 2.1 and 4.8 mg m<sup>-3</sup> for the miniDOAS and the CRDS, respectively. The background  
 210 concentration for V-CH and VI-CH was the same since they were carried out on the same day (see Table  
 211 1).



212  
 213 *Figure 1 – Position of the orifices of the artificial source, ultrasonic anemometer (sonic), and the*  
 214 *concentration analyzer used in the eight controlled release experiments (CRE) of this study. Three*  
 215 *types of analyzers have been used: cavity ring-down spectrometer (CRDS), GasFinder (GF) and*  
 216 *miniDOAS (MD). The arrow indicates the wind direction during each experiment.*

217 In Denmark, the three wind components were measured at 16 Hz with a 3D ultrasonic anemometer  
 218 (WindMaster, Gill, Hampshire, UK) at 1.5 and 1.7 m height. In addition to concentration and wind, air  
 219 temperature, and atmospheric pressure were also measured. In Switzerland, the wind components were  
 220 measured at 20 Hz with a 3D ultrasonic anemometer (WindMaster, Gill, Hampshire, UK) at 2 m height.

221 Air temperature and atmospheric pressure were obtained from a meteorological station nearby the  
222 experiment site.

223 A Global Positioning System (in Denmark: GPS Trimbel R10, Sunnyvale, California, USA; in  
224 Switzerland: GPS Trimble Pro 6, Sunnyvale, California, USA) was used to record the position of all  
225 instruments and the individual critical orifices of the source.

## 226 2.5 Inverse dispersion method

227 The measured gas emission rates (Q) from the artificial source were calculated in 15 min  
228 (experiments conducted in Denmark) or 10 min average intervals (experiments conducted in Switzerland)  
229 using the R (R Core Team, 2018) package bLSmodelR (<https://github.com/ChHaeni/bLSmodelR>;  
230 version 4.3) as described by Häni et al. (2018). The simulation was performed with six million backward  
231 trajectories (N) and the source area defined as 24 individual circles of 5 cm radius as described by Häni et  
232 al. (2018) with a high performance computer cluster (PRIME - Programming Rig for Modern  
233 Engineering, Aarhus University).

234 The emissions rate (Q) is proportional to the difference between measured concentration downwind  
235 ( $C_{\text{downwind}}$ ) from the source and the measured background concentration ( $C_{\text{upwind}}$ ), and the dispersion  
236 factor (D):

$$Q = \frac{C_{\text{downwind}} - C_{\text{upwind}}}{D} \quad (1)$$

237 The dispersion factor (D) is calculated as:

$$D = \frac{1}{N} \sum_{\text{TDinside}} \left| \frac{2}{w_{\text{TD}}} \right| \quad (2)$$

238 where N is the number of backward trajectories from the downwind analyzer location. The  
239 summation refers to the trajectories touching inside the source area (TDinside) taking the vertical

240 velocity( $w_{TD}$ ) at touchdown into account. The calculation of D includes determination of wind profiles  
241 and turbulence statistics that are based on the Monin-Obukhov Similarity Theory (MOST).

## 242 2.6 Surface deposition velocity

243 Ammonia is a relatively short lived gas in the atmosphere and can either be chemically converted, or  
244 subjected to dry or wet deposition. Dry deposition of  $NH_3$  is a complex mechanism that is restricted by  
245 both, atmospheric dispersion towards, and uptake at surfaces (thus, is correlated to several different  
246 conditions indicated by e.g. wind speed, solar radiation, vegetation reactivity). The dry  $NH_3$  deposition  
247 rate is often expressed with a deposition velocity ( $v_d$ ). In this study, we model dry deposition as a canopy  
248 resistance ('big-leaf') approach where  $v_d$  takes place uni-directionally and it is calculated with the canopy  
249 resistances (Hicks et al., 1987):

$$v_d = \frac{1}{R_a + R_b + R_c} \quad (3)$$

250 where  $R_a$  is the aerodynamic resistance,  $R_b$  is the quasi-laminar boundary resistance and  $R_c$  is the bulk  
251 canopy resistance. Because  $R_a$  (the resistance between the concentration measurement height and the  
252 notional height  $z_0$ ) is already included in the bLS model calculations, Eq. 3 can be simplified to represent  
253 a surface deposition velocity:

$$v_d^* = \frac{1}{R_b + R_c} \quad (4)$$

254 For each model trajectory calculation, this surface deposition velocity is acting on each touchdown  
255 outside the emitting source to provide individual dry deposition fluxes  $F_d$  from prevailing touchdown  
256 concentration  $C_{TD}$  as:

$$F_d = -v_d^* C_{TD} \quad (5)$$

257 This reduces the modelled trajectory concentration at each touchdown outside the source by:

$$\Delta C_d = C_{TD} * \left( \exp \left( -\frac{2 * v_d^*}{w_{TD}} \right) - 1 \right) \quad (6)$$

258 We refer to Häni et al. (2018) for the derivation of the above equation and a thorough explanation of  
259 the implementation of the dry deposition algorithm in the bLS model.

260 In this study,  $R_b$  was calculated according to Garland (1977), as a function of the roughness length  
261 ( $z_0$ ), the friction velocity ( $u^*$ ), the kinematic viscosity of air ( $\nu$ ) and the molecular diffusivity of  $NH_3$  in  
262 air ( $\delta_{NH_3}$ ):

$$R_b = \frac{1.45 \left( \frac{z_0 u^*}{\nu} \right)^{0.24} \left( \frac{\nu}{\delta_{NH_3}} \right)^{0.8}}{u^*} \quad (7)$$

263 Regarding  $R_c$ , it is related to the chemical characteristics of the studied gas and the characteristics of  
264 the leaf (e.g. type, size). There are different models to calculate  $R_c$ . Due to the complexity and the  
265 uncertainty of the determination of the resistance,  $R_c$  was calculated following the same procedure as by  
266 Häni et al. (2018) with the bLSmodelR. It was assumed that  $Q_{bLS}/Q < 1$  was solely due to dry deposition.  
267 A similar approach is used here, where 12 values of  $R_c$  from 0 to  $500 \text{ s m}^{-1}$  were tested in the bLS model  
268 that includes ammonia deposition to estimate the  $R_c$  giving  $Q_{bLS}/Q = 1$  in all intervals. This was done with  
269 linear interpolation between the two points closest to  $Q/Q = 1$ . Using this estimated  $R_c$  and the calculated  
270  $R_b$  value for each interval,  $v_d^*$  was estimated for all intervals with all instruments. The  $v_d^*$  values are  
271 compared to previously reported values for  $NH_3$ .

272 Another approach for calculating the  $R_c$  is with an empirical equation, which will be used for  
 273 calculating values for  $v_d^*$ . These calculated values will be compared to the values obtained with the bLS  
 274 model. It is assumed that  $R_c$  is unidirectional and equal to the sum of the stomatal resistance  $R_s$  and the  
 275 cuticular resistance  $R_w$ , see Eq.6.

$$\frac{1}{R_c} = \frac{1}{R_s} + \frac{1}{R_w} \quad (8)$$

276 The stomatal resistance  $R_s$  is calculated with equation Eq.7 (Wesely, 2007):

$$R_s = R_{s(\min)} \left[ 1 + \left( \frac{200}{SR + 0.1} \right) \right]^2 \frac{400}{T_s(40 - T_s)} \quad (9)$$

277 where  $R_{s(\min)}$  is minimum bulk canopy  $R_s$  for water vapour that is assumed to be equals to 250 s  
 278  $m^{-1}$  (Lynn and Carlson, 1990), SR is the solar radiation, and  $T_s$  is the soil temperature.

279 The cuticular resistance is calculated with Eq. 8 (Massad et al., 2010):

$$R_w = \frac{R_{w(\min)} e^{a(100-RH)} e^{0.15T}}{(LAI)^{0.5}} \quad (10)$$

280 where  $R_{w(\min)}$  is the minimum cuticular resistance,  $a$  is an empirical factor, RH is the relative  
 281 humidity,  $T$  is the air temperature, and LAI is the leaf area index. The parameters  $R_{w(\min)}$  ( $10 \text{ s m}^{-1}$ ),  $a$   
 282 ( $0.110$ ) and LAI ( $2 \text{ m}^2 \text{ m}^{-2}$ ) were obtained from Massad et al., 2010, Table 1.

### 283 **3 Results and discussion**

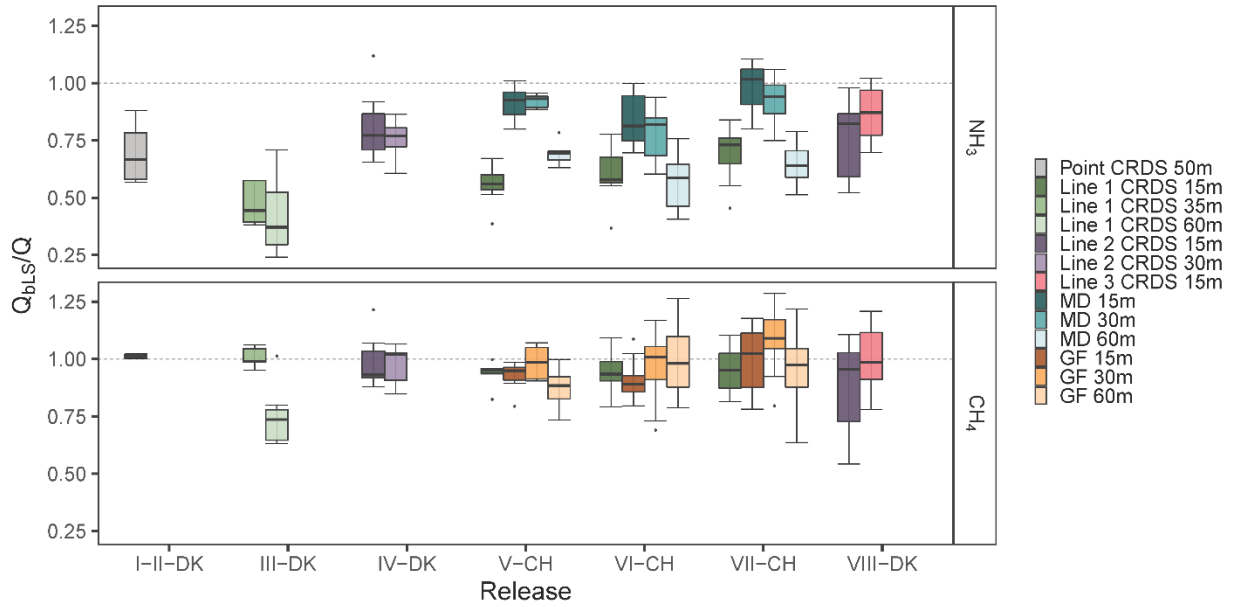
#### 284 **3.1 Recovered fractions of Ammonia and Methane**

285 The accuracy of the bLS model is evaluated by the recovered  $\text{NH}_3$  and  $\text{CH}_4$  fractions,  $Q_{\text{bLS}}/Q$ , and  
 286 the standard deviation  $\sigma_{Q_{\text{bLS}}/Q}$  for all the releases without taking  $\text{NH}_3$  deposition into account. In all  
 287 experiments except I-DK and II-DK (Table 1),  $\text{NH}_3$  and  $\text{CH}_4$  were released simultaneously. The use of

288 these two gases give us the additional opportunity to assess potential loss of NH<sub>3</sub> downwind from the  
289 source by deposition or gas-to-particle conversion, processes that will not occur for CH<sub>4</sub> due to its  
290 inertness. As the average of all releases and measurement systems, the CH<sub>4</sub> recovery rate was  $0.95 \pm 0.08$   
291 ( $n = 19$ ) (Figure 4). This recovery is similar to  $0.93 \pm 0.14$  ( $n = 8$ ) observed by Gao et al. (2008) with a  
292 different controlled releases configuration and ground-level sources. There was more variation in the  
293 recovery of NH<sub>3</sub>, with an average of  $0.66 \pm 0.15$  ( $n = 10$ ) for all the releases with the line-integrated  
294 system. However, the improved sampling lines (Line 2 and 3) placed at 15 m downwind from the source  
295 had an average recovery of  $0.82 \pm 0.05$  ( $n = 3$ ) for NH<sub>3</sub> (Figure 2). Under comparable conditions, the NH<sub>3</sub>  
296 recovery rate obtained with the miniDOAS (MD) was  $0.91 \pm 0.07$  ( $n = 3$ ). Häni et al. (2018) observed  
297 almost the same recovered fraction,  $0.91 \pm 0.12$ , at 15 m from the edge of the source with the MD. The  
298 recovery rates of all experiments in this study are shown in Figure 2, whereas climate conditions such as  
299 wind direction, friction velocity  $u_*$ , air temperature, relative humidity (RH), soil temperature and solar  
300 radiation (SR) from each experiment are presented in Supplementary Information, Table S2. In addition,  
301 the average of the recovery fraction rates of both gases and their relation in each release are shown in  
302 Table 2. I-DK and II-DK were conducted during cold conditions ( $\sim 5^\circ\text{C}$ ) with RH ranging from 65 % to  
303 71 %, whereas IV-DK and VIII-DK were conducted in warm conditions (14 – 18°C) with RH between 48  
304 % and 63 %. The other releases were conducted under moderate temperature conditions (10 – 13°C) with  
305 RH between 39% and 89%.

306 Additional information on the atmospheric conditions, weather conditions, and recovery fraction  
307 rates for each average time interval for each release are shown in Table S1 in the Supplementary  
308 Information.





309

310 *Figure 2 .- The recovered fractions  $Q_{bLS}/Q$  of ammonia and methane from each release and analyzer. The*  
 311 *downwind distance from the source to the analyzer is indicated in the legend. Line 1 had a length of 16 m,*  
 312 *and it was heated to 40 °C. Line 2 had the same temperature as Line 1, but it was 12 m long. Line 3 had*  
 313 *the same length as Line 2, but was heated to 80 °C. Error bars represent the standard deviation.*

314

315

316

317

318

319

320

321

322  
323  
324

Table 2 – Average of the recovery fractions  $Q_{\text{bLS}}/Q$  of ammonia and methane for each release and analyzer with standard deviation. Line 1, Line 2, and Line 3 are described in the Figure 2 caption.

Release	Analyzer and distance	$Q_{\text{bLS}}/Q_{\text{NH}_3}$	$Q_{\text{bLS}}/Q_{\text{CH}_4}$	$Q_{\text{NH}_3}/Q_{\text{CH}_4}$
I-DK	Point CRDS 50m	0.70±0.15		
II-DK	Point CRDS 50m		1.01±0.02	
III-DK	Line 1 CRDS 35m	0.47±0.09	1.01±0.05	0.47±0.21
III-DK	Line 1 CRDS 60m	0.42±0.17	0.75±0.13	0.57±0.44
IV-DK	Line 2 CRDS 15m	0.81±0.16	0.99±0.12	0.82±0.23
IV-DK	Line 2 CRDS 30m	0.76±0.08	0.97±0.08	0.78±0.14
	Line 1 CRDS 15m	0.53±0.11	0.92±0.07	0.57±0.23
V-CH	MD, GF 15m	0.90±0.08	0.91±0.08	0.99±0.13
	MD, GF 30m	0.91±0.05	0.98±0.07	0.92±0.09
	MD, GF 60m	0.68±0.05	0.80±0.23	0.86±0.30
	Line 1 CRDS 15m	0.60±0.10	0.95±0.09	0.63±0.20
VI-CH	MD, GF 15m	0.84±0.11	0.90±0.09	0.93±0.16
	MD, GF 30m	0.78±0.12	0.97±0.16	0.80±0.22
	MD, GF 60m	0.57±0.12	1.00±0.15	0.57±0.26
	Line 1 CRDS 15m	0.69±0.12	0.95±0.10	0.73±0.20
VII-CH	MD, GF 15m	0.98±0.10	0.99±0.15	0.99±0.18
	MD, GF 30m	0.92±0.10	1.08±0.15	0.85±0.17
	MD, GF 60m	0.64±0.09	0.95±0.18	0.68±0.23
VIII-DK	Line 2 CRDS 15m	0.77±0.17	0.89±0.20	0.86±0.31
VIII-DK	Line 3 CRDS 15m	0.87±0.11	1.00±0.14	0.86±0.19

325

### 326 3.2 Sampling systems for closed-path measurement

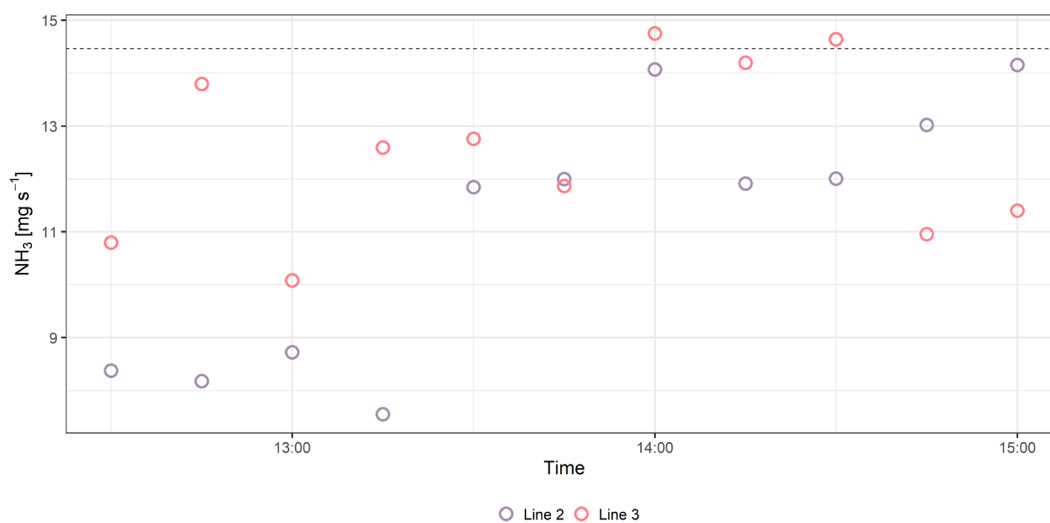
327 Three different CRDS sampling line systems have been used from III-DK to VIII-DK. The difference  
328 between the lines was the length and the heating temperature. Line 1 had a length of 16 m, and it was heated  
329 to 40 °C. Line 2 had the same temperature as Line 1, but it was 12 m long. Line 3 had the same length as  
330 Line 2, but was heated to 80 °C, and the critical orifices have a higher inflow than Line 1 and Line 2 (see  
331 section 2.4 Set-up). We expect that decreasing the length and increasing the heating temperature of the line  
332 will improve  $Q_{\text{bLS}}/Q$  for  $\text{NH}_3$  (no expected effect for  $\text{CH}_4$ ) by avoiding adsorption and reducing the response  
333 time in the sampling line.

334 Line 1 was used with the source at ground level and elevated (Table 1), whereas the other two lines  
335 only with the source elevated. When the source was at ground level, Line 1 had a recovery rate ranging  
336 from  $0.42 \pm 0.17$  to  $0.60 \pm 0.10$  and from  $0.75 \pm 0.13$  to  $1.01 \pm 0.05$  for  $\text{NH}_3$  and  $\text{CH}_4$ , respectively. The  
337 lowest and the highest  $\text{NH}_3$  recovery rate of Line 1 are directly related to the furthest (60 m) and the shortest  
338 (15 m) downwind distance measurement from the source. In addition, the standard deviation  $\sigma_{Q_{\text{bLS}}/Q}$  at the  
339 furthest position is higher than at the closest position, which is in accordance with the results from Häni et  
340 al. (2018). High uncertainty of the  $Q_{\text{bLS}}/Q$  is related to a smaller difference in concentration between  
341 downwind and background concentrations and due to smaller D-values (Häni et al., 2018). This is also the  
342 reason for the low  $\text{CH}_4$  recovery rate of Line 1 in III-DK at 60 m ( $0.75 \pm 0.13$ ), downwind concentration is  
343 only 4 – 10% higher than upwind concentrations since this is one of the lowest  $\text{CH}_4$  releases rate (Table 1).  
344 This is in line with Coates et al. (2021), who observed that the bLS model underestimated 49% of  $\text{CO}_2$   
345 released at 50 m fetch distance partially because the measured downwind concentration was close to the  
346 background level. Therefore, in this study, the accuracy of  $Q_{\text{bLS}}$  is mainly influenced by the uncertainty of  
347 the concentration measurement, hence the downwind distance is limited by the properties of the gas  
348 analyzers and the size of the emission strength of the source. This means the system can be limited in use  
349 if the emission source has a large height and low emission strength where, as a rule of thumb, measurements  
350 should be conducted at a distance from the source at least 10 times the height of the source (Harper et al.,  
351 2011).

352 In VII-CH, Line 1 was used with the source elevated and had a recovery rate of  $0.69 \pm 0.12$  for  $\text{NH}_3$   
353 and  $0.95 \pm 0.10$  for  $\text{CH}_4$ . Line 2 had a numerically higher recovery rate than Line 1, ranging from  $0.76 \pm$   
354  $0.08$  to  $0.81 \pm 0.16$  and from  $0.89 \pm 0.20$  to  $0.99 \pm 0.12$  for  $\text{NH}_3$  and  $\text{CH}_4$ , respectively in IV-DK and VIII-  
355 DK. The length of the line appears to affect the  $\text{NH}_3$  recovery rate; this might be due to the increased surface  
356 area that  $\text{NH}_3$  can adsorb to, and there is a lower flow in each of the critical orifices that decreases the  
357 response time of the system (Shah et al., 2006; Vaittinen et al., 2014). Looking at the measured  $\text{NH}_3$  rates  
358 over time (Figure 3), higher emissions are reached with Line 3 for the first hour indicating a faster time

359 response compared to Line 2. However, after an hour there was not a clear difference between the lines.  
 360 The results indicate that increasing the sampling line temperature to 80 °C had a positive effect on the  
 361 recovery, which reached 87 % at a distance of 15 m. From the data obtained by the open-path analyzer  
 362 (MD), we can conclude that deposition can cause a reduction in recovery in the order of 2-16% (Figure 2).  
 363 Thus, the recovery obtained with the improved line (Line 3) approaches the recovery obtained with the  
 364 open-path analyzer. It should be noted that a direct comparison between Line 3 and the open-path analyzer  
 365 (MD) has not been made and further improvement can still be suggested for the CRDS sampling line  
 366 system. Specifically, increasing the flow through the sampling line and critical orifices will reduce NH<sub>3</sub>  
 367 adsorption in the tubing material. However, similar flow rates through the sampling orifices in the sampling  
 368 line must still be ensured.

369

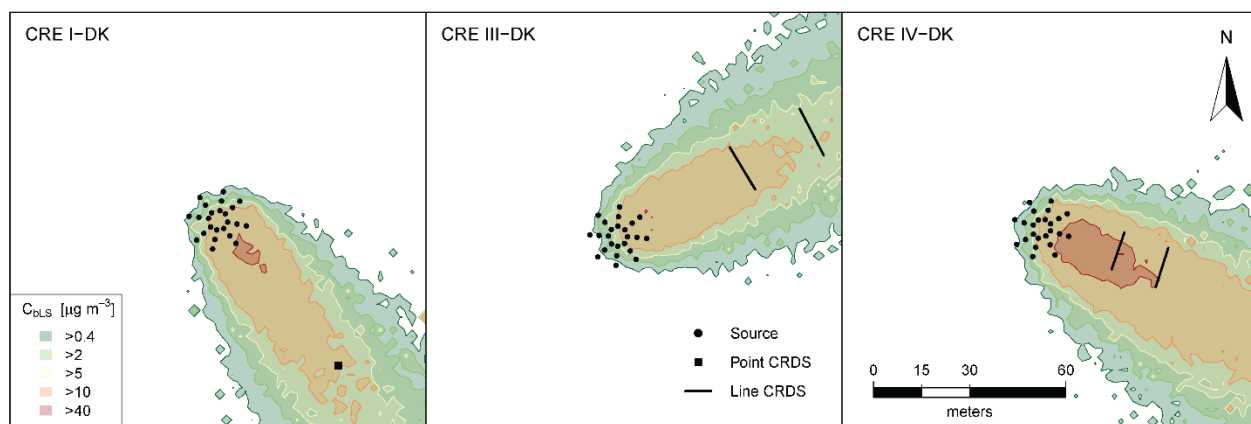


370

371 *Figure 3 .- Ammonia (NH<sub>3</sub>) fluxes measured with Line 2 and Line 3 in 10 min intervals average in VIII-*  
 372 *DK.*

373 The point CRDS system had a recovery rate of  $0.70 \pm 0.22$  and  $1.01 \pm 0.05$  for NH<sub>3</sub> and CH<sub>4</sub>,  
 374 respectively. The benefit of the point CRDS system is mainly that increasing the flow in the tubing is less  
 375 limited, since there are no critical orifices for which equal flow must be maintained. However, comparing  
 376 point and line CRDS systems by the modelled concentration distribution (Figure 4), the line-integrated  
 377 measurement system covers a larger part of the emission plume from the source in a higher wind direction

378 range. In addition, a line-integrated measurement system can reduce uncertainty in the IDM (Flesch et al.,  
 379 2004), since it is less sensitive to error in the measured wind direction. This is in accordance with Ro et  
 380 al. (2011), who observed an almost double recovery value of a line-integrated measurement system for  
 381 CH<sub>4</sub> compared to a point measurement system using a photoacoustic gas monitor.



382

383 *Figure 4.- Contours of the modelled concentration distribution ( $C_{bLS}$ ) for CRE I-DK, CRE III-DK and*  
 384 *CRE IV-DK.*

### 385 3.3 Open-path measurement systems

386 The recovery rates for the GFs (CH<sub>4</sub>) ranged from  $0.87 \pm 0.10$  to  $1.08 \pm 0.15$ . In V-CH to VII-CH,  
 387 the corresponding standard deviation  $\sigma_{Q_{bLS}/Q}$  of GF 15 m varies from 0.07 to 0.18, while Line 1 (placed  
 388 parallel to GF 15 m) ranges from 0.06 to 0.10. These standard deviations  $\sigma_{Q_{bLS}/Q}$  are comparable with  
 389 those measured by Gao et al. (2009) ( $1.03 \pm 0.16$ ).

390 In V-CH and VI-CH (source at ground), the MDs (NH<sub>3</sub>) had recovery rates ranging from  $0.57 \pm$   
 391  $0.12$  to  $0.93 \pm 0.03$ . In VII-CH, MDs exhibit higher recoveries ranging from  $0.64 \pm 0.09$  to  $0.98 \pm 0.10$   
 392 since the source was elevated. Generally, it is recommended to do a release experiment above ground  
 393 level to reduce the probability of deposition close to the release area (McBain and Desjardins, 2005b). As  
 394 expected, the recovery rate decreased with downwind distance of the sampling position due to NH<sub>3</sub>  
 395 deposition, which will be evaluated in section 3.4. Comparing MD at 15 m and Line 1 (placed in parallel)  
 396 in V-CH to VII-CH (Figure 2), the recovery rates are higher for MD. The highest difference between MD

397 and Line 1 was in V-CH, where there were the highest RH (87%). However, there are no clear patterns  
398 explaining the difference between emissions from the different measurement systems based on  
399 atmospheric conditions (Supplementary Information, Figure S2). Although, the improved recovery with  
400 Line 2 ( $0.81 \pm 0.16$ ) and Line 3 ( $0.87 \pm 0.11$ ) in IV-DK and VIII-DK could be influenced by the warmer  
401 conditions and solar radiation (Supplementary Information, Table S2), it is plausible that the line  
402 improvements caused the increase. An increased flow through the orifices and higher temperature of the  
403 sampling line will lead to less  $\text{NH}_3$  adsorption thereby getting a better recovery from the release.

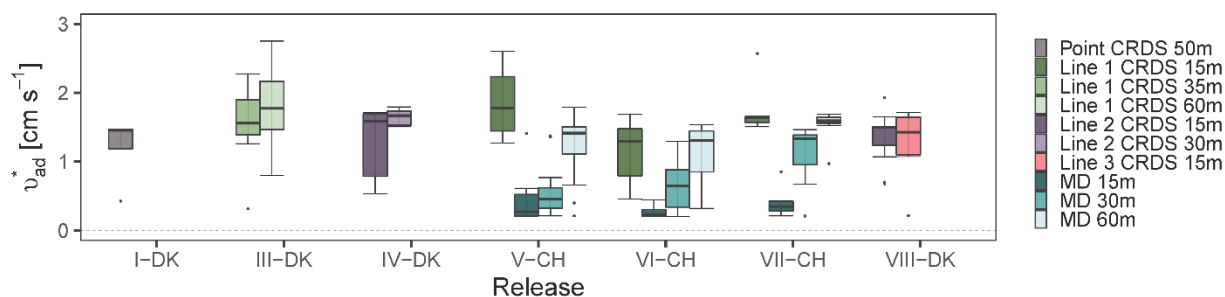
404 These results show the advantage of an open-path instrument compared to a closed-path instrument  
405 to measure  $\text{NH}_3$  emissions (Figure 2), since open-path avoids prolonged response caused by the  
406 adsorption of  $\text{NH}_3$  to sampling materials (Shah et al., 2006; Vaittinen et al., 2014). However, quality  
407 assurance is more challenging for open-path instruments because the use of a closed gas cell for  
408 calibration with a certified gas standard is tedious and means that the instrument setup deviates  
409 significantly from field measurement (DeBruyn et al., 2020). Intercomparison to a reference method (as  
410 an alternative to gas standard calibration) may also introduce uncertainties (Häni et al., 2021). In  
411 addition, the closed-path system presented in this study (line CRDS) is more flexible with respect to  
412 moving the sampling line around the source depending on the predominant wind direction. This is  
413 particularly important in areas with frequently changing wind direction.

#### 414 3.4 Surface deposition velocity

415 The corresponding surface deposition velocities ( $v_d^*$ ) required to have a recovery rate  $Q_{\text{bLS}}/Q =$   
416  $Q_{\text{CH}_4}$  are presented in Figure 5. This approach assumes a recovery equals to the measured  $Q_{\text{CH}_4}$  for each of  
417 the measurement systems when taking deposition into account, which is not completely correct for  
418 closed-path sampling. In the following, therefore, we refer to deposition velocity required to achieve  
419  $Q_{\text{bLS}}/Q = Q_{\text{CH}_4}$  as the *apparent* deposition velocity ( $v_{\text{ad}}^*$ ). This is included to provide data on deposition  
420 velocities for ammonia for which data is currently very limited. The recovery rates observed in Figure 2

421 show that the MD performed best, whereas lower  $Q_{bLS}/Q$  were seen in the sampling lines, thus the lowest  
 422  $v_{ad}^*$  is expected from MD. Additional information of  $R_c$  and  $v_{ad}^*$  for each time intervals in each  
 423 experiment is shown in Table S1 in the Supplementary Information. The apparent surface deposition  
 424 velocities ranged from 0.2 to 1.8  $\text{cm s}^{-1}$  for open-path data and from 0.2 to 4.2  $\text{cm s}^{-1}$  for the line  
 425 sampling. Häni et al. (2018) reported  $v_{ad}^*$  in the range from 0.3 to 1.1  $\text{cm s}^{-1}$ . In all the releases where  
 426 downwind concentrations were measured at different positions,  $v_{ad}^*$  appears to increase with distance. For  
 427 example, in VI-CH,  $v_{ad}^*$  is  $0.3 \pm 0.1$ ,  $0.7 \pm 0.4$  and  $1.1 \pm 0.5$   $\text{cm s}^{-1}$  at 15 m, 30 m and 60 m, respectively.  
 428 The reason for this increase with distance is presently unclear and should be investigated further.

429 In V-CH, VI-CH and VII-CH,  $v_{ad}^*$  from Line 1 are 4.9, 4.3 and 4.3 times higher than MD at 15 m.  
 430 As expected  $v_{ad}^*$  was higher for Line 1 as the  $Q/Q$  was lower for Line 1 compared to MD in these  
 431 experiments. Comparing the apparent deposition velocities from these experiments show comparable  
 432 values for Lines 2 and 3, but higher values for Line 1, i.e. Line 1 (VII-CH) had  $v_{ad}^*$  of  $1.7 \pm 0.4$ , whereas  
 433 Line 2 and Line 3 (VIII-DK) had  $v_{ad}^*$  of  $1.4 \pm 0.4$  and  $1.2 \pm 0.6$   $\text{cm s}^{-1}$ , respectively, when measuring 15  
 434 m from the elevated source. During VII-CH and VIII-DK the temperature differed  $1^\circ\text{C}$  and the relative  
 435 humidity was approximately the same, but wind speed and solar radiation differed (Supplementary  
 436 Information, Table S2).

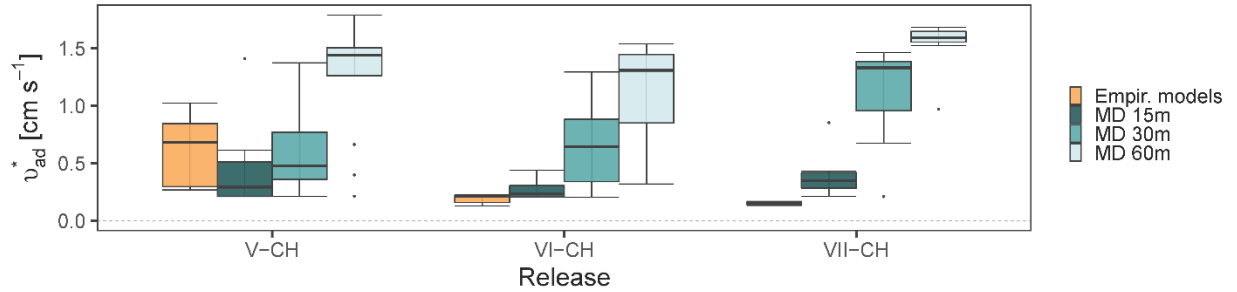


437  
 438 *Figure 5 .- Corresponding apparent surface deposition velocities ( $v_{ad}^*$ ) required to have a recovery rate*  
 439  *$Q_{bLS}/Q$  closest to 1 in all the releases. The error bars represent the standard deviations. All values are*  
 440 *shown in Table S1 in the Supplementary Information.*

441 Many factors affect the deposition velocity, but it is possible to calculate  $v_{ad}^*$  from empirical  
442 models as explained previously (see section 2.6). Figure 6 shows  $v_{ad}^*$  for MDs in V-CH, VII-CH, and  
443 VIII-CH compared to  $v_{ad}^*$  calculated with the empirical models (equations 3-8). Using the empirical  
444 models,  $v_{ad}^*$  varies from 0.13 to 1.02  $\text{cm s}^{-1}$ , increasing with the relative humidity (87%, 76% and 52%  
445 RH in V-CH, VI-CH and VII-CH, respectively). The difference between the two ways of estimating  $v_{ad}^*$   
446 is not surprising since: i) bLS-derived deposition may be influenced by methodological uncertainties and  
447 therefore deviate from true deposition, ii) calculated resistances are associated with uncertainties due to  
448 estimations of physical parameters. In addition, an artificial source most likely will have higher  $v_{ad}^*$  than  
449 what is expected from a typical agricultural source (Häni et al., 2018). This is expected because an  
450 artificial source with discrete outlets located near the ground will have a larger deposition close to the  
451 release because the ground has a high capacity for  $\text{NH}_3$  sorption. On the contrary, a constantly and  
452 homogeneously emitting source (e.g. storage tank or manure pile) is not expected to have any significant  
453 deposition within the source. This is seen with the higher  $v_{ad}^*$  values found in these experiments  
454 compared to the calculated values with the empirical models. The height of the source might also have an  
455 influence on  $v_{ad}^*$ . This is indicated by the lowest  $v_{ad}^*$  in VII-CH, where the source was elevated compared  
456 to V-CH and VI-CH, where the gas was released on the surface. Placing the source above ground level  
457 will reduce the obstacles (crop on the field) for gas dispersion, reducing surface deposition. However, the  
458 bLS model does not consider the height of the source. For example, evaluating emissions from the  
459 application of liquid animal manure (ground level source) or a dairy housing (elevated source) will have  
460 different  $v_{ad}^*$ .

461





462

463 *Figure 6.- Corresponding apparent surface deposition velocities ( $v_{ad}^*$ ) required to have a recovery*  
 464 *rate  $Q_{bLS}/Q$  closest to 1 for miniDOAS (MD) in release V-CH, VI-CH and VII-CH and  $v_{ad}^*$  calculated*  
 465 *with an empirical models.*

466

### 467 3.5 Uncertainties and sensitivity analysis

468 The line-integrated concentration measurement systems with a CRDS analyzer (Line 1, Line 2, and  
 469 Line 3; excluding one value at 60 m) had an average recovery rate of CH<sub>4</sub> of 96%±4% (1 standard  
 470 deviation, n =8) (see also Table 2). Based on this, it is concluded that the method is not biased with  
 471 respect to CH<sub>4</sub>. The overall precision of CH<sub>4</sub> concentration measurements observed for the three versions  
 472 of the line ranged from 4% to 22% at 15 m distance (see Table 2). The equivalent precision for NH<sub>3</sub>  
 473 concentration measurements was between 13% and 23% (Table 2) for the improved sampling lines (Line  
 474 2 and Line 3) at 15 m distance (CRE IV and CRE VIII). The 9% difference between NH<sub>3</sub> recovery rates  
 475 for MD (CRE V-CH – VII-CH) and for Line 2-3 at 15m distance is assessed to represent the sampling  
 476 line adsorption bias related to the line-integrated system under the best conditions (improved sampling  
 477 lines and moderate to warm temperatures). The most relevant factors affecting the uncertainties are the  
 478 determination of the wind direction offset, canopy height and downwind concentration analyzer height.  
 479 Furthermore, the accuracy of the concentration measurements and data filtering criteria related to the  
 480 meteorological conditions (e.g., Flesch et al., 2005) are other important factors that influence the  
 481 uncertainty of the measurement. It would require a comprehensive study to evaluate the contributions of  
 482 these parameters, which is not the scope of this study. Therefore, only sensitivity analyses of the wind

483 direction offset and the sensor height are included below. The individual uncertainty contributions would  
484 be lumped into the overall precision and bias mentioned above.

485 A sensitivity analysis of two input parameters for the bLS model was based on the resulting Q/Q  
486 ratio when changing the inlet height of the analyzer and the wind direction offset compared to the valid  
487 measured values in release VIII-DK. This was done for 11 fluxes in average intervals of 15 min, where all  
488 emissions were estimated again with the bLS model. For the assessment of the influence of the input for  
489 the measurement height all other variables were kept constant. Likewise, for the influence of the wind  
490 direction, all other variables were kept constant while the wind direction offset was changed. The results  
491 are presented in Figure S4 in the Supplementary Information, where it can be seen that Q/Q was most  
492 sensitive to the changes in wind direction offset, stressing the importance of the true offset in wind  
493 direction. Therefore, the wind direction must be thoroughly evaluated for the accuracy of emission  
494 estimation since more or less trajectories have touchdowns inside of the source area for the dispersion  
495 factor (Eq. 2). In addition, the uncertainty of Q/Q ratio increases as wind direction offset increases. The  
496 emission estimation accuracy from point systems is more sensitive to error in the measured wind direction  
497 (Flesch et al., 2004).

498 The accuracy and precision of the emission estimation also depends on the detection limits of the  
499 concentration sensor analyzer, especially when the downwind concentration is close to the background  
500 level, as it was shown previously (see section 3.2). Therefore, it is recommended to conduct concentration  
501 and turbulence measurements not far from the source but minimum 10 times the source height according  
502 to Harper et al. (2011) at a known height to reduce the uncertainty of the calculated emissions rates.

## 503 **4 Conclusion**

504 Line-average concentration measurement with a closed-path analyzer is comparable with an open-  
505 path system, as the average of all releases with all instrument types, the CH<sub>4</sub> recovery rate  $Q_{\text{bLS}}/Q$  was  
506  $0.95 \pm 0.08$  ( $n = 19$ ). Under comparable conditions, average recovery rates of  $0.82 \pm 0.05$  ( $n = 3$ ) and 0.91

507  $\pm 0.07$  ( $n = 3$ ) for  $\text{NH}_3$  and  $0.94 \pm 0.02$  ( $n = 3$ ) and  $0.93 \pm 0.05$  ( $n = 3$ ) for  $\text{CH}_4$  were obtained with the  
508 closed-path and open-path line integrated system, respectively. The implementation of the new method  
509 presented in this study will enable measurement of fluxes of multiple gases from different type of sources  
510 and evaluate the effects of mitigation strategies on emissions. In addition, this method allows for  
511 continuous online measurements that resolve temporal variation in  $\text{NH}_3$  emissions and the peak emissions  
512 of  $\text{CH}_4$ . It is stressed that the wind direction must be thoroughly evaluated for the accuracy of emission  
513 estimation with the bLS model.

514 A significant fraction of the emitted  $\text{NH}_3$  is deposited near the source. Consequently, including the  
515 deposition algorithm in the bLS model will have less bias in the emission evaluation at ground level  
516 sources (e.g. application of liquid animal manure), compared to elevated sources (e.g. slurry tank). The  
517 present study shows that the estimated deposition velocities are in the same order of magnitude in all the  
518 releases with some variation across the different approaches (instrument, distance, method).

## 519 **Acknowledgments**

520 This study was funded by the Ministry of the Environment and Food of Denmark as a service  
521 agreement 2019-760-001136. Thanks to Simon Bowald for his great ideas and his help with designing  
522 and building up the Line 3. Thanks to Marcel Bühler for his valuable contribution in creating some  
523 figures for this paper. Also thanks to technicians Martin Häberli-Wyss, Peter Storegård Nielsen, Jens  
524 Kristian Kristensen, and Heidi Grønbæk for their invaluable help during the experimental part of the  
525 study. We thank the reviewers for valuable comments that helped to improve the article.

## 526 **References**

527 2016/2284/EU, n.d. Directive (EU) 2016/2284 of the European Parliament and of the Council of  
528 14 December 2016 on the reduction of national emissions of certain atmospheric pollutants,  
529 amending Directive 2003/35/EC and repealing Directive 2001/81/EC.

530 Aneja, V.P., Schlesinger, W.H., Erisman, J.W., 2009. Effects of Agriculture upon the Air Quality  
531 and Climate: Research, Policy, and Regulations. *Environmental Science & Technology* 43,  
532 4234–4240. <https://doi.org/10.1021/es8024403>

533 Bai, M., Loh, Z., Griffith, D.W.T., Turner, D., Eckard, R., Edis, R., Denmead, O.T., Bryant,  
534 G.W., Paton-Walsh, C., Tonini, M., McGinn, S.M., Chen, D., 2022. Performance of open-path  
535 lasers and Fourier transform infrared spectroscopic systems in agriculture emissions research.  
536 *Atmos. Meas. Tech.* 15, 3593–3610. <https://doi.org/10.5194/amt-15-3593-2022>

537 Baldé, H., VanderZaag, A.C., Burt, S., Evans, L., Wagner-Riddle, C., Desjardins, R.L.,  
538 MacDonald, J.D., 2016a. Measured versus modeled methane emissions from separated liquid  
539 dairy manure show large model underestimates. *Agriculture, Ecosystems & Environment* 230,  
540 261–270. <https://doi.org/10.1016/j.agee.2016.06.016>

541 Baldé, H., VanderZaag, A.C., Burt, S.D., Wagner-Riddle, C., Crolla, A., Desjardins, R.L.,  
542 MacDonald, D.J., 2016b. Methane emissions from digestate at an agricultural biogas plant.  
543 *Bioresource Technology* 216, 914–922. <https://doi.org/10.1016/j.biortech.2016.06.031>

544 Baldé, H., VanderZaag, A.C., Burt, S.D., Wagner-Riddle, C., Evans, L., Gordon, R., Desjardins,  
545 R.L., MacDonald, J.D., 2018. Ammonia emissions from liquid manure storages are affected by  
546 anaerobic digestion and solid-liquid separation. *Agricultural and Forest Meteorology* 258, 80–88.  
547 <https://doi.org/10.1016/j.agrformet.2018.01.036>

548 Bühler, M., Häni, C., Ammann, C., Mohn, J., Neftel, A., Schrade, S., Zähler, M., Zeyer, K.,  
549 Brönnimann, S., Kupper, T., 2021. Assessment of the inverse dispersion method for the  
550 determination of methane emissions from a dairy housing. *Agricultural and Forest Meteorology*  
551 307, 108501. <https://doi.org/10.1016/j.agrformet.2021.108501>

552 Carozzi, M., Loubet, B., Acutis, M., Rana, G., Ferrara, R.M., 2013. Inverse dispersion modelling  
553 highlights the efficiency of slurry injection to reduce ammonia losses by agriculture in the Po  
554 Valley (Italy). *Agricultural and Forest Meteorology* 171–172, 306–318.  
555 <https://doi.org/10.1016/j.agrformet.2012.12.012>

556 Coates, T.W., Alam, M., Flesch, T.K., Hernandez-Ramirez, G., 2021. Field testing two flux  
557 footprint models. *Atmos. Meas. Tech.* 14, 7147–7152. <https://doi.org/10.5194/amt-14-7147-2021>

558 DeBruyn, Z.J., Wagner-Riddle, C., VanderZaag, A., 2020. Assessment of Open-path  
559 Spectrometer Accuracy at Low Path-integrated Methane Concentrations. *Atmosphere* 11, 184.  
560 <https://doi.org/10.3390/atmos11020184>

561 Delre, A., Mønster, J., Samuelsson, J., Fredenslund, A.M., Scheutz, C., 2018. Emission  
562 quantification using the tracer gas dispersion method: The influence of instrument, tracer gas  
563 species and source simulation. *Science of The Total Environment* 634, 59–66.  
564 <https://doi.org/10.1016/j.scitotenv.2018.03.289>

565 Desjardins, R.L., Denmead, O.T., Harper, L., McBain, M., Massé, D., Kaharabata, S., 2004.  
566 Evaluation of a micrometeorological mass balance method employing an open-path laser for  
567 measuring methane emissions. *Atmospheric Environment* 38, 6855–6866.  
568 <https://doi.org/10.1016/j.atmosenv.2004.09.008>

569 EEA, 2019. EMEP/EEA air pollutant emission inventory guidebook 2019: technical guidance to  
570 prepare national emission inventories. Publications Office, LU.

571 FAO, 2017. Food and Agriculture Organization of the United Nations. The future of food and  
572 agriculture: trends and challenges. Food and Agriculture Organization of the United Nations,  
573 Rome.

574 Flesch, T., Wilson, J., Harper, L., Crenna, B., 2005. Estimating gas emissions from a farm with  
575 an inverse-dispersion technique. *Atmospheric Environment* 39, 4863–4874.  
576 <https://doi.org/10.1016/j.atmosenv.2005.04.032>

577 Flesch, T.K., Desjardins, R.L., Worth, D., 2011. Fugitive methane emissions from an agricultural  
578 biodigester. *Biomass and Bioenergy* 35, 3927–3935.  
579 <https://doi.org/10.1016/j.biombioe.2011.06.009>

580 Flesch, T.K., McGinn, S.M., Chen, D., Wilson, J.D., Desjardins, R.L., 2014. Data filtering for  
581 inverse dispersion emission calculations. *Agricultural and Forest Meteorology* 198–199, 1–6.  
582 <https://doi.org/10.1016/j.agrformet.2014.07.010>

583 Flesch, T.K., Wilson, J.D., Harper, L.A., Crenna, B.P., Sharpe, R.R., 2004. Deducing Ground-to-  
584 Air Emissions from Observed Trace Gas Concentrations: A Field Trial. *Journal of Applied*  
585 *Meteorology* 43, 487–502. <https://doi.org/10.1175/JAM2214.1>

586 Flesch, T.K., Wilson, J.D., Harper, L.A., Todd, R.W., Cole, N.A., 2007. Determining ammonia  
587 emissions from a cattle feedlot with an inverse dispersion technique. *Agricultural and Forest*  
588 *Meteorology* 144, 139–155. <https://doi.org/10.1016/j.agrformet.2007.02.006>

589 Flesch, T.K., Wilson, J.D., Yee, E., 1995. Backward-Time Lagrangian Stochastic Dispersion  
590 Model and Their Application to Estimate Gaseous Emissions. *Journal of Applied Meteorology*  
591 34, 1320–1332. <https://doi.org/10.1175/1520-0450>

592 Fredenslund, A.M., Rees-White, T.C., Beaven, R.P., Delre, A., Finlayson, A., Helmore, J., Allen,  
593 G., Scheutz, C., 2019. Validation and error assessment of the mobile tracer gas dispersion  
594 method for measurement of fugitive emissions from area sources. *Waste Management* 83, 68–78.  
595 <https://doi.org/10.1016/j.wasman.2018.10.036>

596 Gao, Z., Desjardins, R.L., Flesch, T.K., 2009. Comparison of a simplified micrometeorological  
597 mass difference technique and an inverse dispersion technique for estimating methane emissions  
598 from small area sources. *Agricultural and Forest Meteorology* 149, 891–898.  
599 <https://doi.org/10.1016/j.agrformet.2008.11.005>

600 Gao, Z., Desjardins, R.L., van Haarlem, R.P., Flesch, T.K., 2008. Estimating Gas Emissions  
601 from Multiple Sources Using a Backward Lagrangian Stochastic Model. *Journal of the Air &*  
602 *Waste Management Association* 58, 1415–1421. <https://doi.org/10.3155/1047-3289.58.11.1415>

603 Garland, J.A., 1977. The dry deposition of sulphur dioxide to land and water surfaces. *Proc. R.*  
604 *Soc. Lond. A* 354, 245–268. <https://doi.org/10.1098/rspa.1977.0066>

605 Grant, R.H., Boehm, M.T., Bogan, B.W., 2015. Methane and carbon dioxide emissions from  
606 manure storage facilities at two free-stall dairies. *Agricultural and Forest Meteorology* 213, 102–  
607 113. <https://doi.org/10.1016/j.agrformet.2015.06.008>

608 Hafner, S.D., 2018. The ALFAM2 database on ammonia emission from field-applied manure\_  
609 Description and illustrative analysis. *Agricultural and Forest Meteorology* 14.

610 Häni, C., Bühler, M., Neftel, A., Ammann, C., Kupper, T., 2021. Performance of open-path  
611 GasFinder3 devices for CH<sub>4</sub> concentration measurements close to ambient levels. *Atmos. Meas.*  
612 *Tech.* 14, 1733–1741. <https://doi.org/10.5194/amt-14-1733-2021>

613 Häni, C., Flechard, C., Neftel, A., Sintermann, J., Kupper, T., 2018. Accounting for Field-Scale  
614 Dry Deposition in Backward Lagrangian Stochastic Dispersion Modelling of NH<sub>3</sub> Emissions.  
615 <https://doi.org/10.20944/preprints201803.0026.v1>

616 Harper, L.A., Denmead, O.T., Flesch, T.K., 2011. Micrometeorological techniques for  
617 measurement of enteric greenhouse gas emissions. *Animal Feed Science and Technology* 166–  
618 167, 227–239. <https://doi.org/10.1016/j.anifeedsci.2011.04.013>

619 Harper, L.A., Flesch, T.K., Powell, J.M., Coblenz, W.K., Jokela, W.E., Martin, N.P., 2009.  
620 Ammonia emissions from dairy production in Wisconsin. *Journal of Dairy Science* 92, 2326–  
621 2337. <https://doi.org/10.3168/jds.2008-1753>

622 Harper, L.A., Flesch, T.K., Weaver, K.H., Wilson, J.D., 2010. The Effect of Biofuel Production  
623 on Swine Farm Methane and Ammonia Emissions. *Environmental Quality* 39, 1984–1992.  
624 <https://doi.org/10.2134/jeq2010.0172>

625 Hicks, B.B., Baldocchi, D.D., Meyers, T.P., Hosker, R.P., Matt, D.R., 1987. A preliminary  
626 multiple resistance routine for deriving dry deposition velocities from measured quantities.  
627 *Water Air Soil Pollut* 36, 311–330. <https://doi.org/10.1007/BF00229675>

628 Hu, E., Babcock, E.L., Bialkowski, S.E., Jones, S.B., Tuller, M., 2014. Methods and Techniques  
629 for Measuring Gas Emissions from Agricultural and Animal Feeding Operations. *Critical*  
630 *Reviews in Analytical Chemistry* 44, 200–219. <https://doi.org/10.1080/10408347.2013.843055>

631 Hu, N., Flesch, T.K., Wilson, J.D., Baron, V.S., Basarab, J.A., 2016. Refining an inverse  
632 dispersion method to quantify gas sources on rolling terrain. *Agricultural and Forest*  
633 *Meteorology* 225, 1–7. <https://doi.org/10.1016/j.agrformet.2016.05.007>



634 Kamp, J.N., Chowdhury, A., Adamsen, A.P.S., Feilberg, A., 2019. Negligible influence of  
635 livestock contaminants and sampling system on ammonia measurements with cavity ring-down  
636 spectroscopy. *Measurement Techniques* 12, 2837–2850. [https://doi.org/10.5194/amt-12-2837-](https://doi.org/10.5194/amt-12-2837-2019)  
637 2019

638 Kamp, J.N., Häni, C., Nyord, T., Feilberg, A., Sørensen, L.L., 2021. Calculation of NH<sub>3</sub>  
639 Emissions, Evaluation of Backward Lagrangian Stochastic Dispersion Model and Aerodynamic  
640 Gradient Method 17.

641 Kupper, T., Eugster, R., Sintermann, J., Häni, C., 2021. Ammonia emissions from an uncovered  
642 dairy slurry storage tank over two years: Interactions with tank operations and meteorological  
643 conditions. *Biosystems Engineering* 204, 36–49.  
644 <https://doi.org/10.1016/j.biosystemseng.2021.01.001>

645 Lemes, Y.M., Garcia, P., Nyord, T., Feilberg, A., Kamp, J.N., 2022. Full-Scale Investigation of  
646 Methane and Ammonia Mitigation by Early Single-Dose Slurry Storage Acidification. *ACS*  
647 *Agric. Sci. Technol.* 2, 1196–1205. <https://doi.org/10.1021/acsagscitech.2c00172>

648 Lynn, B.H., Carlson, T.N., 1990. A stomatal resistance model illustrating plant vs. external  
649 control of transpiration. *Agricultural and Forest Meteorology* 52, 5–43.  
650 [https://doi.org/10.1016/0168-1923\(90\)90099-R](https://doi.org/10.1016/0168-1923(90)90099-R)

651 Massad, R.-S., Nemitz, E., Sutton, M.A., 2010. Review and parameterisation of bi-directional  
652 ammonia exchange between vegetation and the atmosphere. *Atmos. Chem. Phys.* 10, 10359–  
653 10386. <https://doi.org/10.5194/acp-10-10359-2010>

654 McBain, M.C., Desjardins, R.L., 2005a. The evaluation of a backward Lagrangian stochastic  
655 (bLS) model to estimate greenhouse gas emissions from agricultural sources using a synthetic  
656 tracer source. *Agricultural and Forest Meteorology* 135, 61–72.  
657 <https://doi.org/10.1016/j.agrformet.2005.10.003>

658 McBain, M.C., Desjardins, R.L., 2005b. The evaluation of a backward Lagrangian stochastic  
659 (bLS) model to estimate greenhouse gas emissions from agricultural sources using a synthetic  
660 tracer source. *Agricultural and Forest Meteorology* 135, 61–72.  
661 <https://doi.org/10.1016/j.agrformet.2005.10.003>

662 McGinn, S.M., Coates, T., Flesch, T.K., Crenna, B., 2008. Ammonia emission from dairy cow  
663 manure stored in a lagoon over summer. *Can. J. Soil. Sci.* 88, 611–615.  
664 <https://doi.org/10.4141/CJSS08002>

665 McGinn, S.M., Flesch, T.K., Beauchemin, K.A., Shreck, A., Kindermann, M., 2019.  
666 *Micrometeorological Methods for Measuring Methane Emission Reduction at Beef Cattle*  
667 *Feedlots: Evaluation of 3-Nitrooxypropanol Feed Additive. J. environ. qual.* 48, 1454–1461.  
668 <https://doi.org/10.2134/jeq2018.11.0412>

669 McGinn, S.M., Flesch, T.K., Crenna, B.P., Beauchemin, K.A., Coates, T., 2007. Quantifying  
670 Ammonia Emissions from a Cattle Feedlot using a Dispersion Model. *J. Environ. Qual.* 36,  
671 1585–1590. <https://doi.org/10.2134/jeq2007.0167>

672 McGinn, S.M., Turner, D., Tomkins, N., Charmley, E., Bishop-Hurley, G., Chen, D., 2011.  
673 *Methane Emissions from Grazing Cattle Using Point-Source Dispersion. J. Environ. Qual.* 40,  
674 22–27. <https://doi.org/10.2134/jeq2010.0239>

675 OECD, FAO, 2019. OECD-FAO Agricultural Outlook 2019-2028, OECD-FAO Agricultural  
676 Outlook. OECD. [https://doi.org/10.1787/agr\\_outlook-2019-en](https://doi.org/10.1787/agr_outlook-2019-en)

677 Pedersen, J.M., Feilberg, A., Kamp, J.N., Hafner, S., Nyord, T., 2020. Ammonia emission  
678 measurement with an online wind tunnel system for evaluation of manure application techniques.  
679 Atmospheric Environment 230, 117562. <https://doi.org/10.1016/j.atmosenv.2020.117562>

680 Platt, U., Stutz, J., 2008. Differential optical absorption spectroscopy: principles and  
681 applications, Physics of Earth and space environments. Springer, Berlin.

682 R Core Team, 2018. R: A language and environment for statistical computing; R Foundation for  
683 Statistical Computing: Vienna, Austria.

684 Ro, K.S., Johnson, M.H., Hunt, P.G., Flesch, T.K., 2011. Measuring Trace Gas Emission from  
685 Multi-Distributed Sources Using Vertical Radial Plume Mapping (VRPM) and Backward  
686 Lagrangian Stochastic (bLS) Techniques. Atmosphere 2, 553–566.  
687 <https://doi.org/10.3390/atmos2030553>

688 Ro, K.S., Stone, K.C., Johnson, M.H., Hunt, P.G., Flesch, T.K., Todd, R.W., 2014. Optimal  
689 Sensor Locations for the Backward Lagrangian Stochastic Technique in Measuring Lagoon Gas  
690 Emission. Journal of Environmental Quality 43, 1111–1118.  
691 <https://doi.org/10.2134/jeq2013.05.0163>

692 Sanz, A., Misselbrook, T., Sanz, M.J., Vallejo, A., 2010. Use of an inverse dispersion technique  
693 for estimating ammonia emission from surface-applied slurry. Atmospheric Environment 44,  
694 999–1002. <https://doi.org/10.1016/j.atmosenv.2009.08.044>

695 Shah, S.B., Grabow, G.L., Westerman, P.W., 2006. Ammonia Adsorption in Five Types of  
696 Flexible Tubing Materials. *Applied Engineering in Agriculture* 22, 919–923.  
697 <https://doi.org/10.13031/2013.22253>

698 Sintermann, J., Ammann, C., Kuhn, U., Spirig, C., Hirschberger, R., Gärtner, A., Neftel, A.,  
699 2011. Determination of field scale ammonia emissions for common slurry spreading practice  
700 with two independent methods. *Atmospheric Measurement Techniques* 4, 1821–1840.  
701 <https://doi.org/10.5194/amt-4-1821-2011>

702 Sintermann, J., Dietrich, K., Häni, C., Bell, M., Jocher, M., Neftel, A., 2016. A miniDOAS  
703 instrument optimised for ammonia field measurements. *Atmospheric Measurement Techniques*  
704 9, 2721–2734. <https://doi.org/10.5194/amt-9-2721-2016>

705 Sommer, S.G., McGinn, S.M., Hao, X., Larney, F.J., 2004. Techniques for measuring gas  
706 emissions from a composting stockpile of cattle manure. *Atmospheric Environment* 38, 4643–  
707 4652. <https://doi.org/10.1016/j.atmosenv.2004.05.014>

708 Todd, R.W., Cole, N.A., Rhoades, M.B., Parker, D.B., Casey, K.D., 2011. Daily, Monthly,  
709 Seasonal, and Annual Ammonia Emissions from Southern High Plains Cattle Feedyards. *J.*  
710 *Environ. Qual.* 40, 1090–1095. <https://doi.org/10.2134/jeq2010.0307>

711 Vaittinen, O., Metsälä, M., Persijn, S., Vainio, M., Halonen, L., 2014. Adsorption of ammonia on  
712 treated stainless steel and polymer surfaces. *Applied Physics B* 115, 185–196.  
713 <https://doi.org/10.1007/s00340-013-5590-3>

714 van Haarlem, R.P., Desjardins, R.L., Gao, Z., Flesch, T.K., Li, X., 2008. Methane and ammonia  
715 emissions from a beef feedlot in western Canada for a twelve-day period in the fall. *Can. J.*  
716 *Anim. Sci.* 88, 641–649. <https://doi.org/10.4141/CJAS08034>

717 VanderZaag, A.C., Flesch, T.K., Desjardins, R.L., Baldé, H., Wright, T., 2014. Measuring  
718 methane emissions from two dairy farms: Seasonal and manure-management effects.  
719 *Agricultural and Forest Meteorology* 194, 259–267.  
720 <https://doi.org/10.1016/j.agrformet.2014.02.003>

721 Vechi, N.T., Mellqvist, J., Scheutz, C., 2022. Quantification of methane emissions from cattle  
722 farms, using the tracer gas dispersion method. *Agriculture, Ecosystems & Environment* 330,  
723 107885. <https://doi.org/10.1016/j.agee.2022.107885>

724 Voglmeier, K., Jocher, M., Häni, C., Ammann, C., 2018. Ammonia emission measurements of  
725 an intensively grazed pasture. *Biogeosciences* 15, 4593–4608. [https://doi.org/10.5194/bg-15-](https://doi.org/10.5194/bg-15-4593-2018)  
726 [4593-2018](https://doi.org/10.5194/bg-15-4593-2018)

727 Wesely, M., 2007. Parameterization of surface resistances to gaseous dry deposition in regional-  
728 scale numerical models☆. *Atmospheric Environment* 41, 52–63.  
729 <https://doi.org/10.1016/j.atmosenv.2007.10.058>

730 Wilson, J.D., Flesch, T.K., Harper, L.A., 2001. Micro-meteorological methods for estimating  
731 surface exchange with a disturbed windflow. *Agricultural and Forest Meteorology* 107, 207–225.  
732 [https://doi.org/10.1016/S0168-1923\(00\)00238-0](https://doi.org/10.1016/S0168-1923(00)00238-0)

733 Yang, W., Que, H., Wang, S., Zhu, A., Zhang, Y., He, Y., Xin, X., Zhang, X., 2019. Comparison  
734 of backward Lagrangian stochastic model with micrometeorological mass balance method for

735 measuring ammonia emissions from rice field. *Atmospheric Environment* 211, 268–273.

736 <https://doi.org/10.1016/j.atmosenv.2019.05.028>

737